NUCL SCI TECH (2017) 28:160
DOI 10.1007/s41365-017-0309-5

Design and calculation of a side-coupled accelerating structure

Ming-Xuan Liu[1] · Cong-Feng Wu[1] · Yun-Gai Tang[1] · Gui-Rong Huang[1]

Received: 23 December 2016 / Revised: 7 April 2017 / Accepted: 11 April 2017 / Published online: 26 October 2017

Abstract In this paper, we present the design and optimization of a side-coupled accelerating structure with an energy switch. The beam parameters are optimized, and the electric field asymmetry in the first cell is analyzed. The new structure we designed has an improvement of 10 times in the accelerating field symmetry. Thermo-mechanical analysis is performed based on the electromagnetic results. The highest temperature is 72.5 °C at the nose cone, and the maximal deformation is 73 µm at the outer edge of the coupling cavity.

Keywords Side-coupled accelerating structure · Energy switch · Beam dynamics · Asymmetry · Thermo-mechanical analysis

1 Introduction

Linac has been widely used for cancer treatment. In China, Tsinghua University and the Beijing Medical Equipment Institute (BMEI) completed an 8–10-MeV traveling-wave linac for medical application in 1998 [1]. And efforts have been made by other groups to produce medical accelerators. According to the World Health Organization, up to 4000 sets of medical accelerators are needed in China [2].

Low-energy linac can treat 85% of the tumors which need radiotherapy. In most cases, electron beams of different energies are required to treat tumors at different depths. This is achieved by an energy switch placed in a side cavity. By changing the device position in the cavity, one can change the field distribution in the accelerating tube [3]. Considering high shunt impedance, good stability and small size, side-coupled accelerating structure is a good candidate for medical use [4]. We designed a side-coupled accelerating structure with an energy switch. According to Ref. [5], the final energies were 6 and 4 MeV. 3D CST microwave studio (MWS) [6] was used for designing the models and ASTRA [7] for simulation of beam dynamics. The design requirements are shown in Table 1.

For side-coupled accelerating structure, the coupling cavity is placed alternately between two accelerating cavities with a magnetic coupling [8]. Due to asymmetry of the structure, the accelerating field will offset from the centerline, resulting in an asymmetric electric field. Especially for electrons of low energies, the electric field symmetry in the first cell is essential. Based on Ref. [9], we done the calculation and improved the structure symmetry.

RF heating should be considered too. The considerable energy dissipation from the nose cones may induce a remarkable temperature rise, causing dangerous thermo-mechanical stress due to the non-uniform temperature distribution [10]. To evaluate this important issue, we performed the thermo-mechanical analysis by ANSYS Workbench [11].

2 Accelerating structure

The compact side-coupled linac is operated on $\pi/2$ mode. It consists of seven accelerating cavities and six coupling cavities. Figure 1 shows the models of

✉ Cong-Feng Wu
cfwu@ustc.edu.cn

Ming-Xuan Liu
liumx@mail.ustc.edu.cn

[1] National Synchrotron Radiation Laboratory, University of Science and Technology of China, Hefei 230029, China

Table 1 Design requirements

Parameters	Values
Frequency (MHz)	2998
Coupling coefficient (%)	3.5
Initial energy (keV)	10
Final energy (MeV)	6 or 4
RMS beam diameter (mm)	< 2

accelerating and coupling cavities with their optimized longitudinal electric field.

To accelerate electrons continuously, the length of each cavity must be $\beta\lambda/2$, where λ is the RF wavelength and $\beta = v/c$ is electron traveling speed over light speed. The accelerating cavity is 50 mm long, while ones of two bunching cavities are 21 and 45 mm, respectively. In order to maximize electric field at the electron bunch entrance, the first accelerating cavity was designed as half-cavity structure. Except the first cell, each accelerating cavity is of a Ω-shape, with a nose cone angle of 20°. The accelerating cavity hole is 4 mm in radius. To meet the requirements of mechanical strength and heat exchange, the web thickness is 3 mm. To get high shunt impendence and Q factor, key parameters of the nose cone are optimized. Resonant frequency of the cavity is fixed at 2998 ± 0.5 MHz [12]. The effective shunt impedance of each accelerating cavity is ~ 100 MΩ/m, and the Q factor of 18,730 and $R/Q = 456$. At the nose cone, the surface electric field reaches s maximized at $E_{max}/E_{average} = 4$, where $E_{average}$ is the average electric field on the axis.

In placing coupling cavities on accelerating cavities, the side-coupled structure operating on $\pi/2$ mode will introduce two periodic units (ACA and CAC, A denotes accelerating cavity and C denotes coupling cavity). The frequency gap of the two units on $\pi/2$ mode is named as stop band. To ensure the whole tube to operate on $\pi/2$ mode, the geometries of ACA and CAC must be adjusted to make the stop band as small as possible [13–15]. The resonant frequency of an optimized accelerating cavity and coupling cavity should be 3021.2 and 3076.9 MHz, respectively, when the coupling coefficient is 3.5%. With coupling slots, the effective shunt impedance of the accelerating cavity will decrease by 3%.

Bi-periodic system has large frequency spaces between operating mode and the adjacent modes [13]. Figure 2a shows the resonant mode ($\pi/2$ mode) of the ACA unit. It can be seen that, on $\pi/2$ mode, there is only little electric field exiting around the coupling slot in the side cavity. The phase shift between two adjacent accelerating cavities is π. Figure 2b shows the model of the whole accelerating cavity.

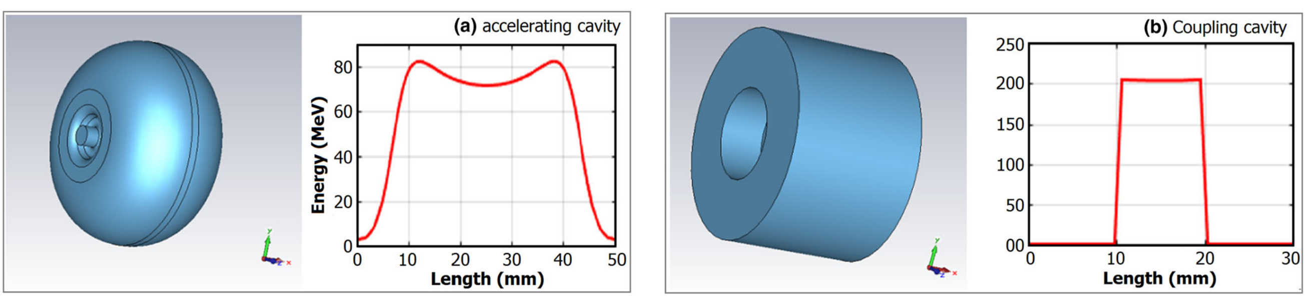

Fig. 1 Models of accelerating (**a**) and coupling cavities (**b**) and their longitudinal electric field curves

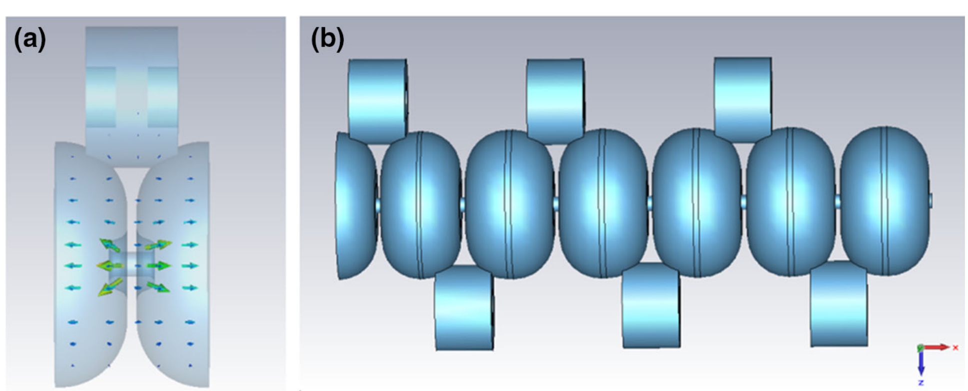

Fig. 2 Electric field profiles of the resonant mode (**a**) and the whole accelerating tube (**b**)

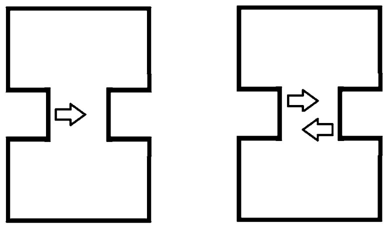

Fig. 3 Schematics of the energy switch

3 Beam dynamics

Two samples of energy switch are shown in Fig. 3. By moving the plunger (s), one can make the coupling unsymmetrical, hence the reduction or increase in electric field downstream. We chose the switch with one plunger [16]. The switch was placed in the fourth coupling cavity.

To calculate the beam dynamics, we converted the accelerating field (calculated by CST) into ASTRA format as its input field file. The effect of space charge was considered in the simulation process. A total of 10,000 macroparticles were used for initial simulations. After scanning all the parameters, full beam dynamics simulation was carried out with 1,000,000 ASTRA macroparticles. The electrons were assumed to be generated from a DC gun. The transverse distribution was radially Gaussian with beam spot size of Φ1 mm (RMS). The longitudinal distribution was uniform with bunch length of 0.7 ns. The initial energy spread and normalized emittance were assumed to be 0.5% and 1.0 π mm mrad, respectively [17–19].

Figure 4a shows the field distributions on the axis when the plunger is 5.21 or 7.91 mm long. At the two positions of the energy switch, the resonant frequencies of the whole structure have a difference of 0.41 MHz. The energy growth curves are shown in Fig. 4b, and the beam sizes at

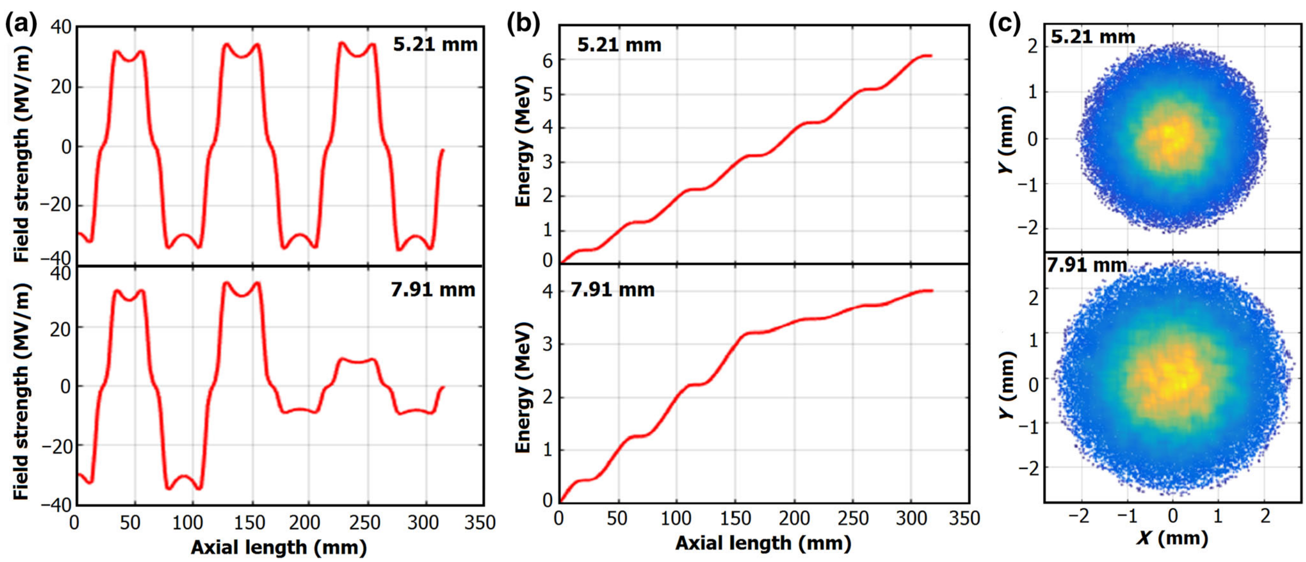

Fig. 4 Longitudinal electric fields of the accelerating tube (**a**), energy growth curves (**b**) and RMS beam bunch diameters (**c**) at different positions of energy switch

Fig. 5 Model of the coaxial coupling cavity (**a**) and electric field distribution in the cavity (**b**)

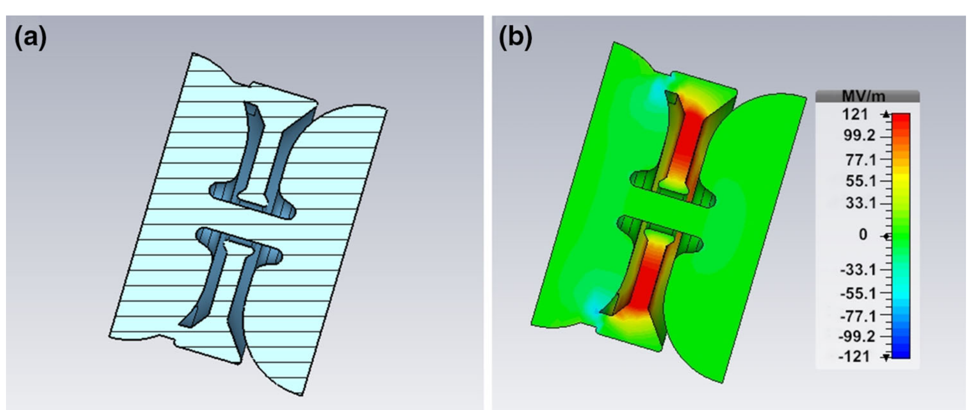

the end of linac are shown in Fig. 4c. Using the electric field (Fig. 4, upper parts), the electrons can be accelerated from 10 to 6081 keV with an average electric field strength of 23.8 MV/m. At the end of accelerating tube, the RMS beam diameter is about 1.42 mm, and the RMS energy spread is 242.7 keV. Using the electric field (Fig. 4, lower parts), the final energy is 4001 keV, with a 0.4-mm increase in RMS beam diameter (which still meets the design requirements) and RMS energy spread of 152.7 keV.

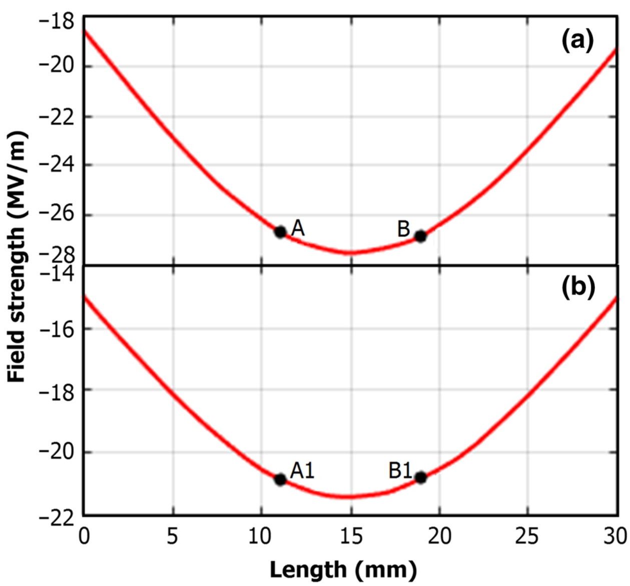

Fig. 6 Symmetry of the prior (**a**) and modified (**b**) structures

4 Asymmetry analysis

To reduce its electric field asymmetry, the first cavity uses coaxial coupling instead. As shown in Fig. 5, by enlarging the regions of the coupling cavity near the outer and inner radii, the magnetic energy is concentrated in the outer and inner regions and the electric energy in the middle region [20]. Coupling is accomplished through a pair of coupling slots 180° apart cut into the web. This preserves symmetry about the beam axis and minimizes the beam perturbation. Further, by rotating the coupling slots 90° at each half of accelerating cavity, the coupling slots are at maximum separation, thereby further reducing the direct coupling between accelerating cavities through the slots.

The longitudinal electric field, which may be expanded into monopole and multi-poles, can be expressed as [21]:

$$E_Z = E_{Z0} + x\Delta E_{\text{d-average}}/(2b), \tag{1}$$

where b is the bore radius and $\Delta E_{\text{d-average}}/(2b)$ is the average amplitude gradient of the dipole electric field. The dipole contribution can be quantified as:

$$\frac{\Delta E_{\text{d}}}{E_Z} = \frac{|E_Z(x = b)| - |E_Z(x = -b)|}{|E_Z(x = 0, y = 0)|}. \tag{2}$$

We calculated $\Delta E_{\text{d}}/E_Z$ of the former structure and the modified it at $b = 4$ mm above and below the axis. The results are shown in Fig. 6. For the former structure, $\Delta E_{\text{d}}/E_Z = 0.698\%$, while it is 0.075% for the optimized structure, i.e., a 10-times improvement in asymmetry of electric field.

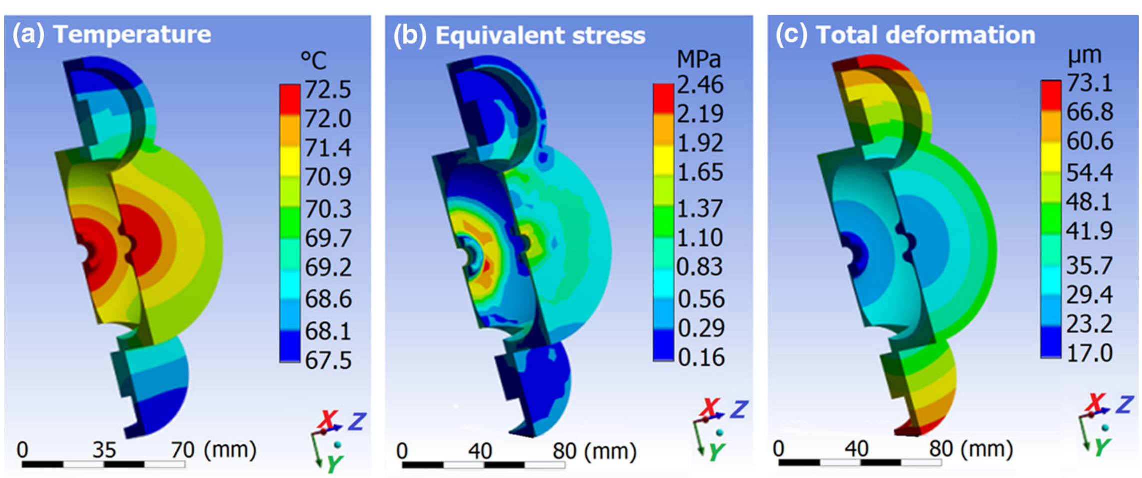

Fig. 7 Thermo-mechanical analysis results

5 Thermo-mechanical analysis

Due to power dissipation in the wall, the structure material is heated by the electromagnetic field. This has a strong impact on the mechanical properties and leads to structure deformation. The loss density (W/m^2) coming from metallic losses can be expressed by [22]:

$$P_{\mathrm{L}} = \frac{R_{\mathrm{S}}}{2} \int |H_{\mathrm{t}}|^2 \mathrm{d}s \tag{3}$$

where P_{L} is the average surface power loss, R_{S} is the surface resistance, and H_{t} is the tangential magnetic field.

We used HFSS module in ANSYS Workbench to calculate the electromagnetic field of one periodic unit (CAC) with copper as the wall material. Then, the electromagnetic results were used to calculate the surface power distribution. The thermo-mechanical analysis was performed, assuming an infinite sequence of accelerating cavities with a boundary condition of perfect insulation [23]. The usual air convection cooling was taken into account. The duty cycle was 2%, and the mesh size of the thermo-mechanical analysis was about 80,000 elements.

The thermo-mechanical analysis results are shown in Fig. 7. The maximum temperature at the nose cone is 72.5 °C. High initial stress is produced at the nose cone and the web where the heat flows away difficultly. Deformation is proportional to the distance to the axis. Maximal deformation of about 73 μm occurs at the outer edge of coupling cavity.

6 Conclusion

The physical calculation and design of a side-coupled accelerating structure have been done. An optimized geometry with high shunt impedance and Q factor was obtained. With the energy switch, the electrons could be accelerated from 10 to 6081 or 4001 keV. The beam characteristics met the design requirements. The accelerating field symmetry in the first cavity was studied, and an optimal design with symmetry improvement of about 10 times was obtained. The thermo-mechanical analysis results of the temperature, equivalent stress and deformation distributions provide estimation for future cooling system.

Acknowledgements The authors would like to thank Guang-Chao Liu, Zhi-Gang He and Biao-Bin Li for helpful discussion. The authors are also grateful to Tong Zhang for technical assistance.

References

1. Y.Z. Lin, Low energy electron linacs and their applications in China, in *Proceeding of the Asian Particle Accelerator Conference, Tsukuba, Japan*, 23–27 Mar 1998
2. R.Y. Song, S.B. He, P. Wang, Development of a 14-MeV dual-mode congeneric mid-energy accelerating structure for medical electron linear accelerator. Nucl. Tech. **39**, 050203 (2016). doi:10.11889/j.0253-3219.2016.hjs.39.050203. **(in Chinese)**
3. S. Hanna, TUPP117: review of energy variation approaches in medical accelerators, in *Proceedings of EPAC08, Genoa, Italy*, 23–27 Jun 2008
4. E.A. Knapp, B.C. Knapp, J.M. Potter, Standing wave high energy linear accelerator structures. Rev. Sci. Instrum. **39**, 979–991 (1968). doi:10.1063/1.1683583
5. X.Q. Lin, P. Zhou, H.B. Zhao et al., Development of side coupled standing wave acceleration tube with energy switch, in *The 7th National Symposium on Medical Accelerator, Tsingtao, China*, 25–28 Sept 2006 (**in Chinese**)
6. CST (Computer Simulation Technology), http://www.cst.com
7. K. Floettmann, ASTRA (A Space Charge Tracking Algorithm), http://www.desy.de/~mpyflo
8. D.E. Nagle, E.A. Knapp, B.C. Knapp, Coupled resonator model for standing wave accelerator tanks. Rev. Sci. Instrum. **38**, 1583–1587 (1967). doi:10.1063/1.1720608
9. E. Tanabe, U.S. Patent 631 6876, High gradient, compact, standing wave linear accelerator structure, 2001
10. S.S. Kurennoy, S. Konecni, J.F. O'Hara et al., THPP027: heating and stress in the lansce side-coupled linac RF cavities, in *Proceedings of EPAC08, Genoa, Italy*, 23–27 Jun 2008
11. ANSYS Workbench, http://www.ansys.com
12. S. Zarei, F.D. Abbasi, S. Ahmadiannamin et al., THPRI040: study of geometrical parameters and their tolerance in optimization of accelerating cells of side coupled linac, in *Proceedings of IPAC2014, Dresden, Germany*, 15–20 Jun 2014
13. T. Nishikawa, S. Giordano, D. Carter, Dispersion relation and frequency characteristics of alternating periodic structure for linear accelerators. Rev. Sci. Instrum. **37**, 652–661 (1966). doi:10.1063/1.1720274
14. H.C. Hoyt, D.D. Simmonds, W.F. Rich, Computer designed 805 MHz proton linac cavities. Rev. Sci. Instrum. **37**, 755–762 (1966). doi:10.1063/1.1720315
15. X.H. Bian, H.B. Chen, S.X. Zheng, Calculation of coupling factor for double-period accelerating structure. High Energy Phys. Nucl. Phys. **29**, 900–902 (2005). doi:10.3321/j.issn:0254-3052.2005.09.015. **(in Chinese)**
16. E. Tanabe, V.A. Vaguine, U.S. Patent 428 6192, Variable energy standing wave linear accelerator structure, 1981
17. R. Dash, A. Sharma, K.C. Mittal, Beam dynamics studies of a 10 MeV standing wave electron linac, in *2014 International Symposium on Discharges and Electrical Insulation in Vacuum, Mumbai, India*. doi:10.1109/DEIV.2014.6961756
18. N. Juntong, R. Chimchang, S. Rimjaem et al., TUPOY015: design of electron gun and S-band structure for medical electron linear accelerator, in *Proceeding of IPAC16, Busan, Korea*, 8–13 May 2016
19. P. Buaphad, H.K. Cha, S. Cha et al., TUPOY010: 6/9 MeV S-band standing wave accelerating structure for container X-ray inspection system at RTX, in *Proceeding of IPAC16, Busan, Korea*, 8–13 May 2016
20. E. Tanabe, M. Bayer, M.E. Trail, U.S. Patent 498 8919, Small-diameter standing-wave linear accelerator structure, 1991
21. M.D. Forno, P. Craievich, G. Penco et al., Theoretical and experimental analysis of a linear accelerator endowed with single

feed coupler with movable short-circuit. Rev. Sci. Instrum. **84**, 114701 (2013). doi:10.1063/1.4827080

22. A. Mahmoud, E.L. Sabbagh, Electromagnetic-thermal analysis study based on HFSS-ANSYS link (Syracuse University, 2011), http://surface.syr.edu/eecs_techreports/46
23. D. Giove, Low energy high power side coupled linac optimization, in *Proceedings of PAC09, Vancouver, Canada*, 4–8 May 2009